Scaling Laws for the Critical Rupture Thickness of Common Thin Films

by

J. E. Coons[1], P. J. Halley[2], S. A. McGlashan[2], and T. Tran-Cong[3]

[1]*Los Alamos National Laboratory, Engineering Sciences and Applications Division, P.O. Box 1663, MS C930, Los Alamos, NM 87545, USA*

[2]*Centre for High Performance Polymers, School of Engineering, University of Queensland, St Lucia, QLD 4072, Australia*

[3]*Department of Mechanical and Mechotronic Engineering, University of Southern Queensland, Toowoomba, QLD 4350, Australia*

Submitting author: J. E. Coons, jimc@lanl.gov, +1-505-667-6362 (Phone), +1-505-665-5548 (Fax)

Abstract. Despite decades of experimental and theoretical investigation on thin films, considerable uncertainty exists in the prediction of their critical rupture thickness. According to the spontaneous rupture mechanism, common thin films become unstable when capillary waves at the interfaces begin to grow. In a horizontal film with symmetry at the midplane, unstable waves from adjacent interfaces grow towards the center of the film. As the film drains and becomes thinner, unstable waves osculate and cause the film to rupture. Uncertainty stems from a number of sources including the theories used to predict film drainage and corrugation growth dynamics. In the early studies, the linear stability of small amplitude waves was investigated in the context of the quasi-static approximation in which the dynamics of wave growth and film thinning are separated. The zeroth order wave growth equation of Vrij predicts faster wave growth rates than the first order equation derived by Sharma and Ruckenstein. It has been demonstrated in an accompanying paper that film drainage rates and times measured by numerous investigations are bounded by the predictions of the Reynolds equation and the more recent theory of Manev, Tsekov, and Radoev. Solutions to combinations of these equations yield simple scaling laws which should bound the critical rupture thickness of foam and emulsion films. In this paper, critical thickness

measurements reported in the literature are compared to predictions from the bounding scaling equations and it is shown that the retarded Hamaker constants derived from approximate Lifshitz theory underestimate the critical thickness of foam and emulsion films. The non-retarded Hamaker constant more adequately bounds the critical thickness measurements over the entire range of film radii reported in the literature. This result reinforces observations made by other independent researchers that interfacial interactions in flexible liquid films are not adequately represented by the retarded Hamaker constant obtained from Lifshitz theory and that the interactions become significant at much greater separations than previously thought.

Keywords: Thin Films, Thinning Velocity, Critical Film Thickness, Spontaneous Rupture Mechanism, Scaling Laws, Lifshitz Theory

1. Introduction

Thin liquid films form between bubbles and droplets in multiphase systems and an improved understanding of their stability and rupture will benefit numerous industries such as tertiary oil exploration, biotechnology, and microchip design and manufacturing [1]. This work is preceded by numerous experimental [2-6] and theoretical [2, 5, 7-10] studies that address film stability and the critical or rupture condition. Despite this wealth of information, significant confusion and uncertainty remains in the ability to predict the critical film thickness from basic physicochemical properties. Uncertainties stem from a number of sources including the underlying theories governing film drainage and wave growth dynamics [11] and the magnitude of the Hamaker constant used to represent the attractive van der Waals forces [12, 13]. The work presented here represents an attempt to bound the prediction of the critical rupture thickness and thereby construct a framework from which past and future thin film studies can be described.

Common thin films rupture via a spontaneous mechanism in which a film becomes unstable when capillary waves at the interfaces begin to grow [7, 10]. The conditions of the onset of instability have been described previously [8, 11]. Unstable capillary waves located along the interfaces of a thin film grow towards the middle of the film, in the direction of the opposing interface. As the film drains and becomes thinner, unstable

waves eventually osculate to rupture the film. Application of the quasi-static approximation allows the rate expressions for film drainage and corrugation growth to be separated in the underlying lubrication theory as a consequence of the vast size difference between the characteristic times of the two phenomena. In this way, approximate equations describing film drainage [11, 14, 15] and corrugation growth [7, 9, 11] have been reported. It was recently demonstrated [16-18], and more thoroughly discussed in an accompanying review paper [19], that the thinning velocities of thin films with suppressed electrostatic interaction and tangentially immobile interfaces can be bounded using the Reynolds equation [10, 14] and the theoretical equation derived by Manev et al [15]. It was also recently shown [17, 18, 20] that the critical thickness of common thin films can be bounded by selectively coupling the drainage equations with the corrugation growth rate expressions derived from linear stability studies. In these previous works, values of the Hamaker constants were taken from a variety of sources. In this study, approximate Lifshitz theory is used throughout to estimate the Hamaker constants for the foam and emulsion film systems and equations from the underlying theory are assembled in such a way as to bound the critical rupture thickness. The resulting scaling equations are then used to explore the consistency of Lifshitz theory and spontaneous rupture theory in predicting the critical rupture thickness of foam and emulsion films.

2. Theory

Lubrication theory describes the squeezing flow of a viscous fluid between two rigid surfaces [14]. This is similar to the thin liquid films that form between bubbles in a foam or droplets in an emulsion. Drainage from the film occurs as a consequence of the pressure drop across the film. When the interfaces are tangentially immobile and nearly plane parallel, lubrication theory is applicable and provides the Reynolds equation for film thinning [10, 11].

$$V_{\mathrm{Re}} = -\frac{dh}{dt} = \frac{2h^3 \Delta P}{3\mu R^2} \tag{1}$$

h is the average film thickness, ΔP is the average radial pressure drop across the film, R is the film radius, and μ is the viscosity of the film. Thin film studies are carried out in specially designed capillary cells in which a thin film forms in the center of the liquid spanning the capillary tube. The Plateau border capillary pressure drop is the pressure

drop at the perimeter of the film due to the curvature of the meniscus. At sufficiently small thicknesses, attractive van der Waals forces acting between the film interfaces increase the intrafilm pressure. The van der Waals forces have a conjoining effect and are included as a negative component of the disjoining pressure. In the absence of electrostatic repulsion, the drainage pressure or average pressure drop across the liquid film is given by the following expression where the first term is the Plateau border pressure drop and the second term is the disjoining pressure.

$$\Delta P = 2\sigma\left(\frac{R_c}{R_c^2 - R^2}\right) + \frac{A}{6\pi h^3} \tag{2}$$

A is the retarded Hamaker constant, R_c is the radius of the capillary tube, and σ is the interfacial tension. Unlike the disjoining pressure component, the Plateau border capillary pressure component is not time dependent as long as the film radius remains constant. The physicochemical parameters and the range of film thickness determine the dominant component of the drainage pressure. Coons et al [11, 19] have shown that for films of large radii, the Plateau border capillary pressure term dominates the drainage pressure throughout the unstable period up to the point of rupture. For small radii films, the disjoining pressure contributes more significantly to the drainage pressure but probably never completely dominates. Domination by the disjoining pressure component throughout the unstable period requires that R be of order h, which violates a basic premise of lubrication theory.

In a free standing liquid film, the interfaces are not rigid and the non-uniform film pressure causes the interface to dimple. Hence, the interfaces become nonparallel as thinning proceeds [1, 5, 15]. The drainage theory of Manev et al [15, 21] assumes that the local film thickness is a homogeneous function of the average film thickness, that the waveform driving the film drainage forms by capillary forces, and that the pressure drop across the corrugated film is directly proportional to the driving pressure divided by the square root of the eigenvalue of the dominant waveform. These assumptions lead to the following expression for the thinning velocity.

$$V = V_{\mathrm{Re}} l^{3/2} \tag{3}$$

l is the number of domains or rings in the film and is given by the following theoretical expression.

$$l = \left[\frac{\Delta P}{h\sigma} \left(\frac{R}{4} \right)^2 \right]^{2/5} \geq 1 \tag{4}$$

Equations (3) and (4) are referred to here as the theoretical MTsR equation. This theory predicts that the number of domains, and hence the thinning velocity ratio, increases as the film thickness decreases. Coons et al [11] obtained the following semi-empirical equation for the number of domains by comparing equation (4) with the thinning velocities reported by Radoev et al [5].

$$l = \frac{1}{2} \left\{ \left[\frac{\Delta P}{h\sigma} \left(\frac{R}{4} \right)^2 \right]^{2/5} + \frac{4}{3} \right\} \geq 1 \tag{5}$$

Equations (3) and (5) are referred to here as the semi-empirical MTsR equation. The theoretical MTsR equation generally predicts higher thinning velocities than the semi-empirical equation. Coons et al [19] have shown that the Reynolds equation typically underestimates thinning velocities, the theoretical MTsR equation consistently overestimates thinning velocities, and the semi-empirical MTsR equation provides more accurate thinning velocities through the stable and unstable periods leading to rupture.

Thin films become unstable when small-amplitude thermal corrugations begin to grow. The linear stability of corrugated films has been investigated in which the dynamics of film thinning and corrugation growth are treated separately [11]. The critical thickness is defined as the optimum average film thickness at rupture, and approximations are obtained by tracking the waveform that is first to reach the center of the film. The amplitude of the critical wave is equivalent to the half film thickness at the critical rupture thickness [2, 9].

$$h_c = 2\zeta_0 \exp(X) \tag{6}$$

ζ_0 is the initial amplitude and is estimated assuming that the corrugation results from thermal motion of the molecules along the interface [5].

$$\zeta_0 = \sqrt{k_B T / \sigma} \tag{7}$$

k_B is Boltzmann's constant and T is absolute temperature. X in equation (6) is the growth constant, which is the dimensionless product of time and the growth rate for the optimum waveform. By replacing time with $\int dh/V$, the growth constant can be

expressed as a function of the film thickness whose form depends on the order of the approximation used to generate the corrugation growth rate. The zeroth order corrugation growth constant [2, 7] neglects the stabilizing effect of film thinning and the destabilizing effect of the film thickness dependency of the Hamaker constant.

$$X_0 = \frac{k_{opt}^2}{24\mu}\int_{h_c}^{h_t}\left[\frac{A}{\pi h} - \sigma k_{opt}^2 h^3\right]\frac{dh}{V} \tag{8}$$

h_c and h_t are the critical and transition thickness of the optimum waveform, respectively. As each waveform has a unique transition and critical thickness, the optimum waveform is the wave that provides the maximum critical thickness and is generally not the first waveform to become unstable. The relationship between the eigenvalue of the optimum waveform $\left(k_{opt}\right)$ and its transition thickness is determined by setting the corrugation growth rate to zero and therefore depends on the order of the corrugation growth rate used. When the zeroth order corrugation growth rate is applied, the eigenvalue of the optimum waveform and its transition thickness have the following relationship.

$$k_{opt} = \left(\frac{A}{\pi\sigma h_t^4}\right)^{1/2} \tag{9}$$

The first order corrugation growth constant [8, 9] and the equation that relates the eigenvalue of the optimum waveform with its transition thickness are provided below.

$$X_1 = X_0 - 3\int_{h_c}^{h_t}\frac{dh}{h} \tag{10}$$

$$k_{opt}^4 - \left(\frac{A}{\pi\sigma h_t^4}\right)k_{opt}^2 + \frac{72\mu V}{\sigma h_t^4} = 0 \tag{11}$$

The first order growth constant includes the stabilizing effect of film thinning but neglects the film thickness dependency of the Hamaker constant. The latter effect is addressed for both corrugation growth constants by employing an effective Hamaker constant described in the subsequent section. The eigenvalue of the optimum waveform is obtained by differentiating equation (6) with respect to k_{opt} and the result is independent of the order of the growth constant used.

$$k_{opt}^2\int_{h_c}^{h_t}\frac{h^3 dh}{V} = \frac{A}{2\pi\sigma}\int_{h_c}^{h_t}\frac{dh}{hV} \tag{12}$$

3. The Hamaker Constant

The equations described in the previous section are dependent on the Hamaker constant, which according to Lifshitz theory is in turn dependent on the dielectric spectrum of the materials in the specific film system as well as the film thickness. As described in an accompanying paper [19], equation 5.9.3 in Russel et al [22] was used to estimate the retarded Hamaker constants for this study. When the film medium contained electrolytes, ion screening of the non-retarded term was included using equations 11.23 and 12.37 from Israelachvili [23]. The equation is based on Lifshitz theory as applied to symmetric films of large lateral dimension (i.e., planar films).

According to Lifshitz theory, the Hamaker constant decreases with increasing film thickness due to retardation effects. This dependency is neglected in the derivation of the above thinning velocity and corrugation growth equations. Given that the difference between the transition and critical rupture thickness of the optimum waveform is relatively small (i.e., approximately 100 Å), application of a film-thickness independent Hamaker constant is appropriate given the approximate nature of the bounding analysis. However, the destabilizing effect of the film thickness dependency of the Hamaker constant requires additional attention. The relative size of the destabilizing effect can be determined by taking the derivative of the disjoining pressure term in equation (2) with respect to *h*. This results in the following effective Hamaker constant.

$$A_{eff}\Big|_h = \left\{1 - \frac{1}{3}\left[\left(\frac{dA}{dh}\Big|_h\right)\left(\frac{h}{A|_h}\right)\right]\right\} A\Big|_h \tag{13}$$

The effective Hamaker constant incorporates the destabilizing effect due to the film thickness dependency of the retarded Hamaker constant on the corrugation growth constant. As shown in Figure 1, the film thickness dependency contribution (i.e., the term in the square brackets in equation (13)) depends on the film thickness as well as the film material but does not fall below -1 for the films considered here. Therefore, the effective Hamaker constant used in this study was taken as the value of the retarded Hamaker constant at the experimentally measured critical film thickness with an approximate film thickness dependency contribution of -1.

$$A_{eff} \approx \frac{4}{3} A\Big|_{h_c} \tag{14}$$

The nonretarded Hamaker constant $\left(A(0)\right)$ was also used in this study and was calculated using equation 5.9.4 from Russel et al [22].

$$A_{131}(0) \approx \frac{3}{4} k_B T \left[\frac{\varepsilon_1(0) - \varepsilon_3(0)}{\varepsilon_1(0) + \varepsilon_3(0)} \right]^2 + \frac{3\hbar\omega}{16\sqrt{2}} \left[\frac{\left(n_1^2 - n_3^2\right)^2}{\left(n_1^2 + n_3^2\right)^{1.5}} \right] \tag{15}$$

The subscript on the Hamaker constant is absent elsewhere in this paper and denotes a film of material 3 with semi-infinite material 1 at each interface. $\hbar$ is Planck's constant (1.0545×10^{-34} Nms/radian), n_i is the refractive index in the visible frequency range of material *i*, $\varepsilon_i(0)$ is the static dielectric constant of material *i*, and ω is the dominant relaxation frequency in radians/s in the ultraviolet frequency range. In the derivation of equation (15), it is assumed that the relaxation frequency is similar in both film materials. However, in practice, this is only approximately correct and in this study the relaxation frequency of the film medium (i.e., material 3) was used. The dielectric and optical properties used to calculate the Hamaker constants, and when available their temperature dependencies, are provided in Table 1. The electrolyte concentrations applied to determine the screening effects in aqueous films are provided in Table 2 along with the calculated effective and nonretarded Hamaker constants.

4. Critical Film Thickness Scaling Laws

For a given drainage velocity expression, the zeroth order growth constant provides higher values of critical thickness than the first order growth constant [11]. Also, the magnitude of the film thickness integral in equation (8) and hence the size of the critical film thickness is inversely proportional to the thinning velocity. Therefore, by combining the Reynolds thinning velocity (equation (1)) and the zeroth order growth constant (equations (8) and (9)) with equations (6), (7), and (12), an upper bound of the critical thickness is obtained. This combination of equations is identical to the theory of Ivanov et al [2]. Previous solutions have been provided [11, 18] with reference to a master curve, which reflects the self-similarity of the film rupture process and is a necessary condition for a scaling law [24]. The master curve elucidates three subdomains over the relevant parameter space whose boundaries are defined by the dominant term in the drainage pressure of equation (2). Approximation of the master

curve by a continuum of three lines, one line for each subdomain, allows the critical thickness to be estimated over the entire relevant parameter space by the following scaling law (see the appendix for an alternate derivation of the basic form of the scaling law).

$$h_c^* = C\left(h_{t,0}^*\right)^x \left(P^*\right)^y \tag{16}$$

h_c^*, $h_{t,0}^*$, and P^* are dimensionless parameters defined as follows.

$$h_c^* = \frac{h_c}{2\zeta_0} \tag{17}$$

$$h_{t,0}^* = \left[\frac{A}{\pi\sigma}\left(\frac{R}{\alpha_{0,1}}\right)^2\right]^{1/4} \Big/ 2\zeta_0 \tag{18}$$

$$P^* = \frac{A\left(R_c^2 - R^2\right)}{12\pi\sigma\left(2\zeta_0\right)^3 R_c} \tag{19}$$

$\alpha_{0,1}$ is the first root of the Bessel function of first kind order zero and has a value of 2.4048. The scaling law constants *C*, *x*, and *y* in equation (16) are dependent on the system of equations solved, the relevant master curve, as well as the subdomain in which a solution is sought. For the system of equations describing the upper bound of the critical thickness, the scaling law constants take on the values provided in **Table** 3. The system of equations representing the upper bound scaling law is identical to the model described by Ivanov et al [2] for stationary films with high concentrations of surfactant when the disjoining pressure is represented as shown in equation (2). Ivanov et al did not provide a general solution in the form of limiting equations, but did show that the model predicted higher than actual critical thickness values for a series of aniline films. Ivanov et al also did not report all of the physicochemical properties necessary to obtain their results, making a quantitative comparison with the scaling laws impossible.

In a similar manner, the scaling law for the lower bound of the critical film thickness was determined. This was accomplished by combining the theoretical MTsR equation (i.e., equations (3) and (4)) and the first order growth constant (equations (10) and (11)) with equations (6), (7), and (12). The resulting lower bound scaling law constants are provided in **Table** 4.

It has been shown that the semi-empirical MTsR equation provides more accurate estimates of the film thinning velocity in the unstable period of a large variety of films [19]. Therefore, combination of the semi-empirical MTsR equation (i.e., equations (3) and (5)) and the zeroth order growth constant (equations (10) and (11)) with equations (6), (7), and (12) may provide more accurate estimates of critical thickness. The scaling law constants for the lower bound of the critical film thickness are provided in **Table 5**.

5. Discussion

The utility of the critical thickness scaling law and the associated constants reported here can be tested by comparing the scaling law predictions with measurements reported in the literature. To meet this objective, critical thickness values reported on a variety of foam and emulsion films were collected [3-7, 25-27]. All of the aqueous films contained sufficient electrolyte to suppress electrostatic repulsion and the interfaces of all of the films were rendered tangentially immobile by the presence of surfactant. The physicochemical properties used for each film in application of the scaling law are provided in Tables 1 and 2. Upper and lower bounds of the critical thickness were calculated using equation (16) with the corresponding constants determined by the drainage pressure condition described in Tables 3 and 4, respectively. Scaling law predictions of the critical thickness bounds in foam and emulsion films using the effective Hamaker constant are compared to the experimentally measured values in Figure 2 and 3. The results demonstrate that only a portion of the foam and emulsion critical thickness measurements are bounded when the effective form of the retarded Hamaker constant is used. For a given film system, the scaling law predicts that the critical film thickness will increase with increasing film radius. This is consistent with the measurements reported in the studies included here. In Figure 2, it is shown that foam films of small radii are bounded by the scaling law predictions whereas the larger films are not. In Figure 3, the no. 6 emulsion films (i.e., tolunen-water-toluene films) of Manev et al [6] are bounded while the other emulsion films are not. The effective Hamaker constant appears to be within a suitable range for smaller films but does not adequately represent the long range van der Waals attraction over the entire size spectrum of foam and emulsion films considered.

It has recently been observed that long range van der Waals forces appear to have a much larger effect in liquid films than is predicted by the retarded Hamaker constant obtained from Lifshitz theory. Sharma et al [13] observed the breakup of micrometer thick polydimethylsiloxane (PDMS) films on solid substrates over time periods that were several orders of magnitude shorter than is predicted by thin film theory. Chen et al [12] independently measured the separation distance at which PDMS or polybutadiene films supported on mica substrates coalesce due to a jump instability created by long range van der Waals attractrive forces. The jump-in distance was measured at around 2000 Å, which is in agreement with theoretical predictions when the non-retarded Hamaker constant is used to represent long range forces. It is therefore of interest to determine if critical film thickness measurements reported in the literature are more globally consistent with the scaling law predictions when the non-retarded Hamaker constants provided in Table 2 are used. Scaling law predictions of the critical thickness bounds in foam and emulsion films using the non-retarded Hamaker constants are compared to the experimentally measured values in Figure 4 and 5. The scaling law bounds are shown to be much more consistent with the experimental measurements. In Figure 4, essentially all of the critical thickness measurements in the foam films are bounded. Also, with the exception of system no. 1 of Traykov et al [3], all of the emulsion films in Figure 5 are shown to be bounded by the scaling law predictions. Emulsion film systems nos. 1 and 4 of Traykov et al contained the same materials but were inverted. That is, film system no. 1 consisted of a benzene film surrounded by water whereas film system no. 4 consisted of a water film surrounded by benzene. According to Lifshitz theory, the Hamaker constants for these two systems are equivalent which is consistent with the Hamaker constants shown in Table 2. However, the critical film thickness measured in system no. 1 was about 35% thicker than in system no. 4. This discrepancy can not be explained by the difference in interfacial tension. The non-retarded Hamaker constant of system no. 4 would have to be increased by a factor of 3 to obtain agreement with the scaling law predictions.

It is of interest to explore this approach when a more accurate film thinning model is coupled with the corrugation growth equation. For this purpose, the semi-empirical MTsR equation was coupled with the zeroth order corrugation growth constant and the resulting scaling law constants are provided in Table 5. The scaling law predictions for both types of films are compared to the actual values in Figure 6 and 7 where the

effective and non-retarded Hamaker constants are used, respectively. Here too, predictions using the non-retarded Hamaker constant more accurately predict the critical film thickness measurements.

6. Conclusions

It is shown in this study that the average critical film thickness of emulsion and foam films can be bounded using a simple scaling law with the constants provided in Tables 3 and 4 when the non-retarded Hamaker constant is employed. The analysis demonstrates general agreement between the predictions of spontaneous rupture theory with the experimental measurements of a broad range of foam and emulsion films based on the growth of the optimum waveform. The equations used in this study only approximate the dynamics of film thinning and corrugation growth in thin films. The scaling laws used to predict bounds for the critical thickness were obtained following a quasi-static approach in which the fastest corrugation growth and slowest film thinning models, or alternatively, the slowest corrugation growth and fastest film thinning models were combined. Although the particular drainage and corrugation growth models in the underlying equations influence the resulting critical thickness predictions, the choice of drainage model appears to have the largest effect. When the scaling law incorporating the more accurate semi-empirical MTsR drainage equation is used, the resulting critical thickness predictions are more accurate for small to moderately sized films. The scaling laws can also be applied to bound the Hamaker constant when accurate critical thickness values are known.

7. Acknowledgements

This work was supported in part by the U. S. Department of Energy under contract W-7405-ENG-36. The authors are grateful to a referee of the original manuscript, who recommended the application of Lifshitz theory to determine the Hamaker constants.

8. Appendix

The basic form of the scaling law can be obtained by assuming that the drainage pressure in equation (2) is dominated by either the Plateau border pressure drop or the disjoining pressure term. Under conditions when the Plateau border pressure drop $\left(P_{\sigma,B}\right)$ dominates and the Reynolds equation is used for film thinning velocities,

equation (12) can be integrated directly. Substitution of equation (9) for k_{opt} provides the following equation relating the critical and transition thicknesses of the optimum waveform.

$$6\left(\frac{h_c}{h_t}\right)^4 = 7\left(\frac{h_c}{h_t}\right)^3 - 1 \tag{A1}$$

Limiting the film thickness ratio to positive values less than 1 provides:

$$\beta = \frac{h_c}{h_t} \approx 0.72 \tag{A2}$$

Integration of the zeroth order corrugation growth constant given by equation (8) followed by substitution of equation (9) provides:

$$X_0 = \frac{A^2R^2}{16\pi^2\sigma P_{\sigma,B}h_t^4}\left[\frac{1}{3}\left(\frac{1}{h_c^3}-\frac{1}{h_t^3}\right)-\frac{\left(h_t-h_c\right)}{h_t^4}\right] \tag{A3}$$

The transition thickness is eliminated by substitution of equation (A2).

$$X_0 = \frac{A^2R^2}{48\pi^2\sigma P_{\sigma,B}h_c^7}\left(1-4\beta^3+3\beta^4\right)\beta^4 \tag{A4}$$

The zeroth order growth rate constant can be rearranged in the form of the dimensionless constants defined in equations (17) through (19). Introducing the resulting growth constant expression into equation (6) provides the following equation for the dimensioless critical film thickness.

$$h_c^* = \exp\left[\frac{\alpha_{0,1}^2\beta^4\left(1-4\beta^3+3\beta^4\right)\left(h_{t,0}^*\right)^4 P^*}{8\left(h_c^*\right)^7}\right] \tag{A5}$$

Taking the natural logarithm of both sides provides the basic form of the scaling law.

$$h_c^* = \left[\frac{\alpha_{0,1}^2\beta^4\left(1-4\beta^3+3\beta^4\right)}{8\ln\left(h_c^*\right)}\right]^{1/7}\left(h_{t,0}^*\right)^{4/7}\left(P^*\right)^{1/7} \tag{A6}$$

The values of the exponents in equation (A6) are approximately equal to the *x* and *y* values listed in the last row of Table 3. The quantity in the square brackets is slightly dependent on the value of the dimensionless critical film thickness, which ranges approximately between 10 and 100. This provides a *C* value that ranges between 0.54 and 0.60. The slightly larger *C* value provided in the last row of Table 3 compensates for the slightly smaller values of *x* and *y*.

A similar approach under conditions where the drainage pressure is dominated by the disjoining pressure provides a β value of 0.67 and equation (A6) becomes:

$$h_c^* = \left\{ \frac{-\alpha_{0,1}^2 \beta^4 \left[\ln \beta + \frac{1}{4}\left(1-\beta^4\right) \right]}{8 \ln\left(h_c^*\right)} \right\}^{1/4} \left(h_{t,0}^*\right) \qquad \text{(A7)}$$

The value of the *x* parameter in the first row of Table 3 is smaller than unity. Although the difference is small, it effectively reduces the value of the critical film thickness by half. The difference is compensated for in the value of the *C* parameter. In equation (A7), the value of *C* ranges between 0.25 and 0.33, which is about half of the value provided in Table 3. The differences between the scaling law parameters provided in this appendix and those in Table 3 are a consequence of the master curve approach described in the previous scaling law section. The master curve approach yields approximate values of the scaling law parameters across the entire range of drainage pressure conditions as well as the approximate boundaries where the various forms of the scaling law are applicable.

Rearrangement of the scaling law into a dimensional form provides an equation that is similar in form to the limiting equations of Vrij [7, 26], which included an undefined parameter (*f*) that was reported to be slightly dependent on film thickness.

9. References

1. I.B. Ivanov and D.S. Dimitrov, Thin Film Drainage, Marcel Dekker, Inc., 1988.
2. I.B. Ivanov, B. Radoev, E. Manev and A. Scheludko, Trans. Faraday Soc., 66 (1970) 1262
3. T.T. Traykov, E.D. Manev and I.B. Ivanov, International Journal of Multiphase Flow, 3 (1977) 485
4. A.A. Rao, D.T. Wasan and E.D. Manev, Chem. Eng. Commun., 15 (1982) 63
5. B.P. Radoev, A.D. Scheludko and E.D. Manev, J. Colloid Interface Sci., 95 (1983) 254
6. E.D. Manev, S.V. Sazdanova and D.T. Wasan, J. Colloid Interface Sci., 97 (1984) 591
7. A. Vrij, Discuss. Faraday Soc., 42 (1966) 23
8. R.J. Gumerman and G.M. Homsy, Chem. Eng. Commun., 2 (1975) 27

9. A. Sharma and E. Ruckenstein, Langmuir, 3 (1987) 760
10. A. Sheludko, Adv. Colloid Interface Sci., 1 (1967) 391
11. J.E. Coons, P.J. Halley, S.A. McGlashan and T. Tran-Cong, Adv. Colloid Interface Sci., 105 (2003) 3
12. N. Chen, T. Kuhl, R. Tadmor, Q. Lin and J.N. Israelachvili, Physical Review Letters, 92 (2004) 024501/1
13. A. Sharma, R. Khanna and G. Reiter, Colloids and Surfaces B: Biointerfaces, 14 (1999) 223
14. O. Reynolds, Philos. Trans. R. Soc. London, 177 (1886) 157
15. E. Manev, R. Tsekov and B. Radoev, J. Dispersion Sci. Technol., 18 (1997) 769
16. J.E. Coons, P.J. Halley, S.A. McGlashan and T. Tran-Cong, Drainage of Emulsion and Foam Films in Scheludko Cells, 5th European Conference on Foams, Emulsions and Applications, Champs-sur-Marne, France, July 2004.
17. J.E. Coons, P.J. Halley, S.A. McGlashan and T. Tran-Cong, Drainage of Emulsion and Foam Films in Scheludko-Exerowa Cells, 21st International Congress of Theoretical and Applied Mechanics, August 2004.
18. J.E. Coons, P.J. Halley, S.A. McGlashan, T. Tran-Cong and A.L. Graham, Bounding the Critical Rupture Thickness of Common Thin Films, 14th International Congress on Rheology, Seoul, Korea, August 2004.
19. J.E. Coons, P.J. Halley, S.A. McGlashan and T. Tran-Cong, Colloids and Surfaces A: Physicochemical and Engineering Aspects, (Submitted 2004)
20. J.E. Coons, P.J. Halley, S.A. McGlashan, T. Tran-Cong and A.L. Graham, Bounding the Critical Rupture Thickness of Common Thin Films, 5th European Conference on Foams, Emulsions and Applications, Champs-sur-Marne, France, July 2004.
21. R. Tsekov, Colloid Surf. A-Physicochem. Eng. Asp., 141 (1998) 161
22. W.B. Russel, D.A. Saville and W.R. Schowalter, Colloidal Dispersions, Cambridge University Press, New York, 1989.
23. J.N. Israelachvili, Intermolecular and Surface Forces, Academic Press, San Diego, 1992.
24. G.I. Barnenblatt, Scaling, Cambridge University Press, Cambridge, United Kingdom, 2003.
25. A. Vrij, Discuss. Faraday Soc., 42 (1966) 60
26. A. Scheludko and E. Manev, Trans. Faraday Soc., 64 (1968) 1123

27. K. Kumar, A.D. Nikolov and D.T. Wasan, J. Colloid Interface Sci., 256 (2002) 194
28. R.C. Weast, Handbook of Chemistry and Physics, CRC Press, Inc., Baco Raton, FL, 1983.

TABLES

Table 1. Dielectric and optical properties[1] of reference film materials.

Material	$\varepsilon(0)$	n	$\omega \times 10^{-16}$ (rad/s)
water	$10^{-0.002(T-298.15)+\log_{10}(78.54)}$	1.333	1.88
air	1.00054	1	-
benzene	$2.284-.002(T-293.15)$	1.5011	1.32
toluene	$2.379-.00243(T-298.15)$	1.474	1.36
chlorobenzene	$10^{-0.0013(T-293.15)+\log_{10}(5.71)}$	1.5241	1.32
aniline	$10^{-0.00148(T-293.15)+\log_{10}(6.89)}$	1.583	1.32

[1] $\varepsilon(0)$ were obtained from Weast [28]. n and ω for water and benzene were obtained from Israelachvili [23]. n and ω for toluene were obtained from reference [19]. The refractive indices for chlorobenzene and aniline were obtained from Weast [28] and the relaxation frequency of benzene was used for both materials.

Table 2. Source of experimental data and the physicochemical properties used for the prediction of critical thickness.

Source of Data and Film Material	Film Type	$\frac{4}{3}A\big\vert_{h_c}\times10^{20}$ (Nm)	$A(0)\times10^{20}$ (Nm)	T (°C)	$\sigma\times10^{3}$ (N/m)	R_c (μm)	R (μm)
Vrij [7]							
air-aniline-air	Foam	2.7	6.5	25[3]	39.4	1840[4]	100
air-water-air	Foam[2]	1.7	3.6	25[3]	65	1790[4]	100
Exerowa & Kolarov (see Vrij [7], page 60)							
air-water-air	Foam[2]	1.2-1.6	3.6	25[3]	55.5	2310[4]	100-400
Scheludko & Manev [26]							
air-chlorobenzene-air	Foam	2.1-3.1	5.5	20	32.6	1140	36-257
air-aniline-air	Foam	2.6-3.7	6.5	20	42.6	1140	36-200
Traykov et al [3]							
water-benzene-water (1)	Emulsion	0.59	0.84	20	28	1350	100
benzene-water-benzene (4)	Emulsion[5]	0.34	1.1	20	34	1450	100
Rao et al [4]							
air-water-air	Foam[6]	1.5-1.7	3.6	25	35	1790	90-140
Radoev et al [5]							
air-water-air	Foam[6]	0.86-1.9	3.6	24	34.5	1790[4]	50-1000
Manev et al [6]							
air-water-air (1)	Foam[6]	1.1-1.9	3.6	25	44.5	1790	50-500
air-water-air (2)	Foam[7]	1.1-1.9	3.6	25	37.0	1790	50-500
air-water-air (3)	Foam[7]	1.1-1.9	3.6	25	34.0	1790	50-500
air-water-air (4)	Foam[7]	1.1-1.9	3.6	25	34.0	1790	50-500
toluene-water-toluene (5)	Emulsion[5]	0.20-0.29	0.86	25	15.0	1580	50-300
toluene-water-toluene (6)	Emulsion[6]	0.20-0.29	0.86	25	7.9	1580	50-300
Kumar et al [27]							
air-water-air	Foam[8]	1.6	3.6	25	37.1	930	178

[2] Aqueous films contained 0.1M KCl.
[3] The temperature was not reported by the data source so the value shown was assumed.
[4] The capillary tube radius was not reported by the data source so the value shown was calculated from the Plateau border pressure drop.
[5] Aqueous films contained 0.3M NaCl.
[6] Aqueous films contained 0.1M NaCl.
[7] Aqueous films contained 0.25M NaCl.
[8] Salt content in the aqueous film is not reported in the reference.

Table 3. Scaling Law Constants for the Upper Bound of the Critical Thickness

$z = P^* \Big/ \left(h_{t,0}^*\right)^{2.861}$	**Dominant Film Pressure Term Throughout Drainage**	C	x	y
$z > 1.239$	Disjoining pressure	0.514	0.944	0
$1.239 > z > 0.0190$	Both disjoining pressure and the Plateau border pressure	0.506	0.735	0.073
$z < 0.0190$	Plateau border pressure drop	0.656	0.548	0.138

Table 4. Scaling Law Constants for the Lower Bound of the Critical Thickness

$z = P^* \Big/ \left(h_{t,0}^*\right)^{2.735}$	**Dominant Film Pressure Term Throughout Drainage**	C	x	y
$z > 1.994$	Disjoining pressure	0.491	0.899	0
$1.994 > z > 0.0172$	Both disjoining pressure and the Plateau border pressure	0.448	0.535	0.133
$z < 0.0172$	Plateau border pressure drop	0.695	0.240	0.241

Table 5. Scaling Law Constants for Intermediate Critical Thickness Values

$z = P^* \Big/ \left(h_{t,0}^*\right)^{2.735}$	**Dominant Film Pressure Term Throughout Drainage**	C	x	y
$z > 1.994$	Disjoining pressure	0.523	0.920	0
$1.994 > z > 0.0172$	Both disjoining pressure and the Plateau border pressure	0.476	0.563	0.133
$z < 0.0172$	Plateau border pressure drop	0.808	0.256	0.241

FIGURE CAPTIONS

Figure 1. The contribution of the film thickness dependency of the retarded Hamaker constant to the effective Hamaker constant as predicted by Lifshitz theory. The value of the bracketed term is shown for benzene, aniline, chlorobenzene, and aqueous films as a function of the film thickness. The contribution is mostly dependent on the film material and not on the material of the surrounding medium. The thickness dependence of benzene films is almost negligible while the contribution in films of the other materials is particularly high when the film thickness is around 1000 Å.

Figure 2. The critical rupture thickness bounds of foam films determined using the effective Hamaker constants in Table 2. The upper (□) and lower (Δ) bounds were determined by the scaling law with constants from Tables 3 and 4, respectively. The size of the critical thickness increases approximately with increasing film radius. Critical film thickness measurements in the smaller films are bounded by the scaling law predictions whereas those in the larger films are not bounded.

Figure 3. The critical rupture thickness bounds of emulsion films determined using the effective Hamaker constants in Table 2. The upper (■) and lower (▲) bounds were determined by the scaling law with constants from Tables 3 and 4, respectively. The size of the critical thickness approximately increases with increasing film radius. Critical film thickness measurements of system no. 6 in Manev et al [6] is the only emulsion film system sufficiently bounded.

Figure 4. The critical rupture thickness bounds of foam films determined using the non-retarded Hamaker constants in Table 2. The upper (□) and lower (Δ) bounds were determined by the scaling law with constants from Tables 3 and 4, respectively. The size of the critical thickness approximately increases with increasing film radius. Critical film thickness measurements over the entire range are bounded by the scaling law predictions.

Figure 5. The critical rupture thickness bounds of emulsion films determined using the non-retarded Hamaker constants in Table 2. The upper (■) and lower (▲) bounds were determined by the scaling law with constants from Tables 3 and 4, respectively. The size of the critical thickness approximately increases with increasing film radius. Critical film thickness measurements for all of the emulsion films are bounded except for system no. 1 emulsion of Traykov et al [3].

Figure 6. The critical rupture thickness of emulsion (■) and foam (□) films determined using the effective Hamaker constants in Table 2 along with the scaling law constants of Table 5. The theoretical values are significantly lower than the experimental measurements.

Figure 7. The critical rupture thickness of emulsion (■) and foam (□) films determined using the non-retarded Hamaker constants in Table 2 along with the scaling law constants of Table 5. The size of the critical thickness approximately increases with increasing film radius. The theoretical predictions deviate more significantly from the measured values with increasing film radius.

FIGURES

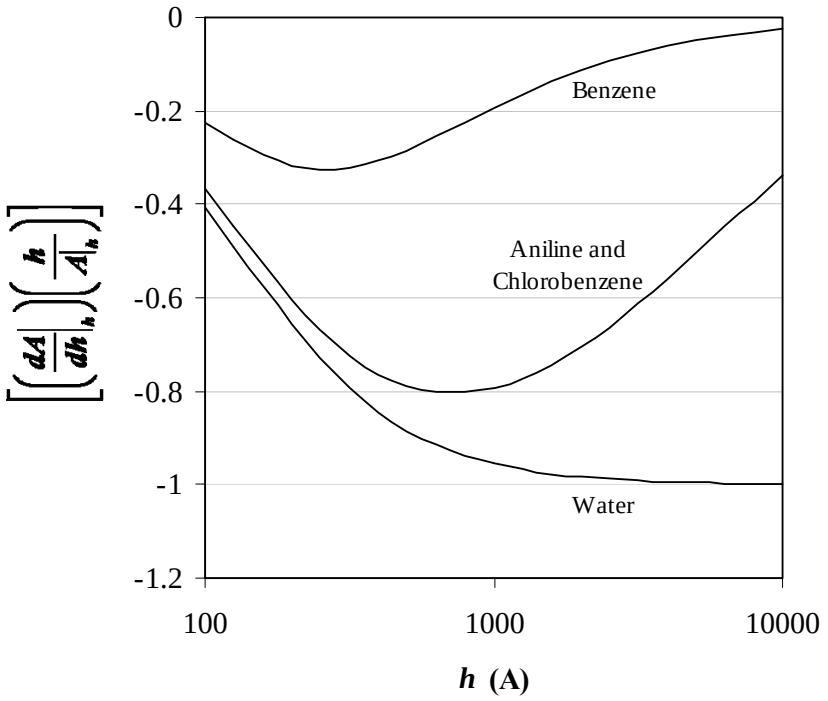

Figure 1.

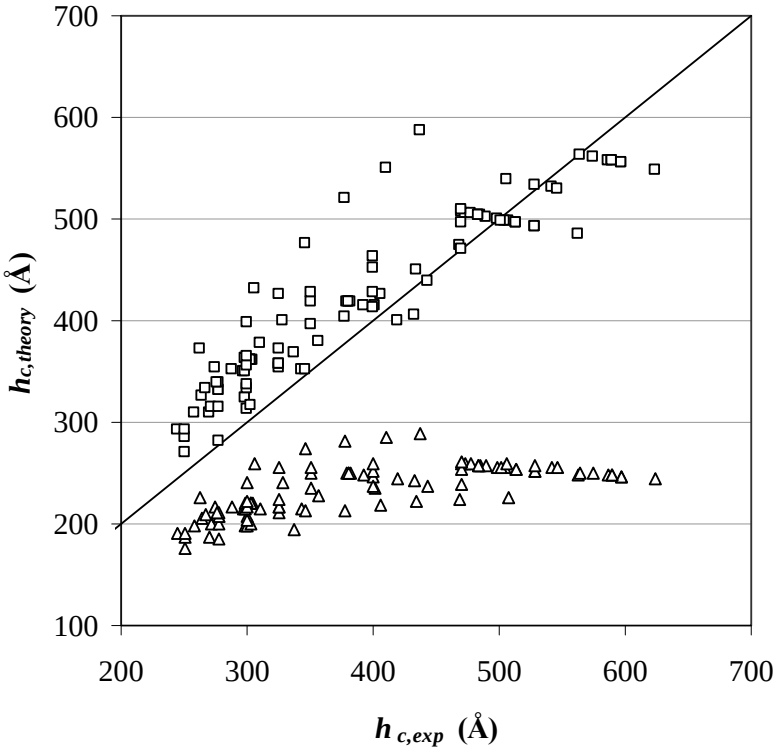
700
600
500
400
300
200
100
200
300
400
500
600
700
$h_{c,theory}$ (Å)
$h_{c,exp}$ (Å)

Figure 2.

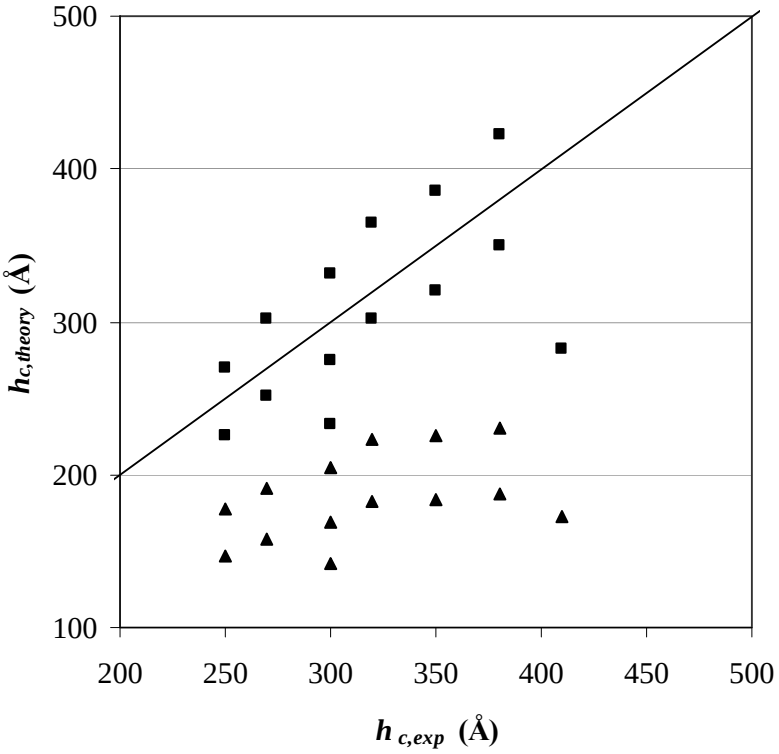
500
400
300
200
100
200
250
300
350
400
450
500
$h_{c,theory}$ (Å)
$h_{c,exp}$ (Å)

Figure 3.

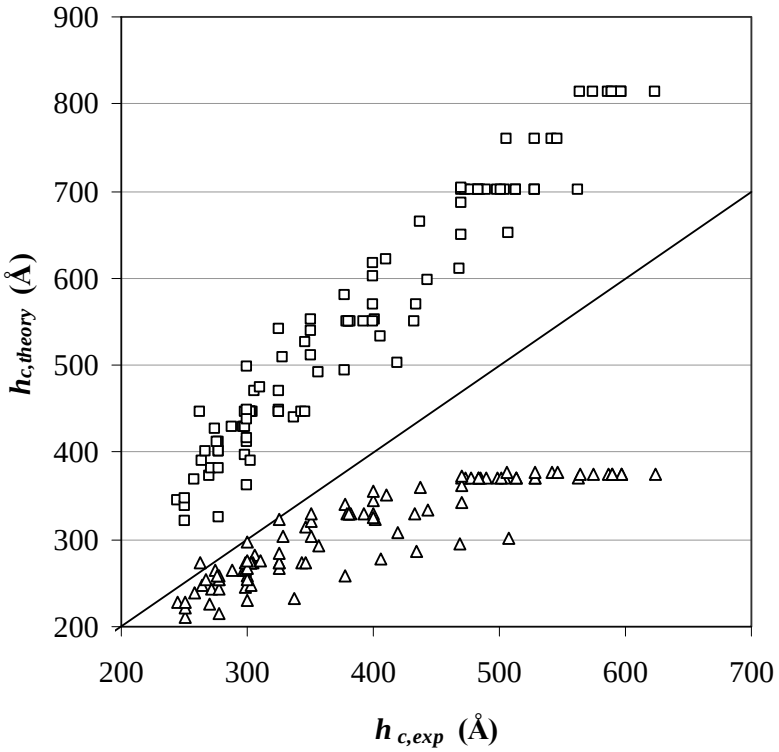
900
800
700
600
500
400
300
200
200
300
400
500
600
700
$h_{c,theory}$ (Å)
$h_{c,exp}$ (Å)

Figure 4.

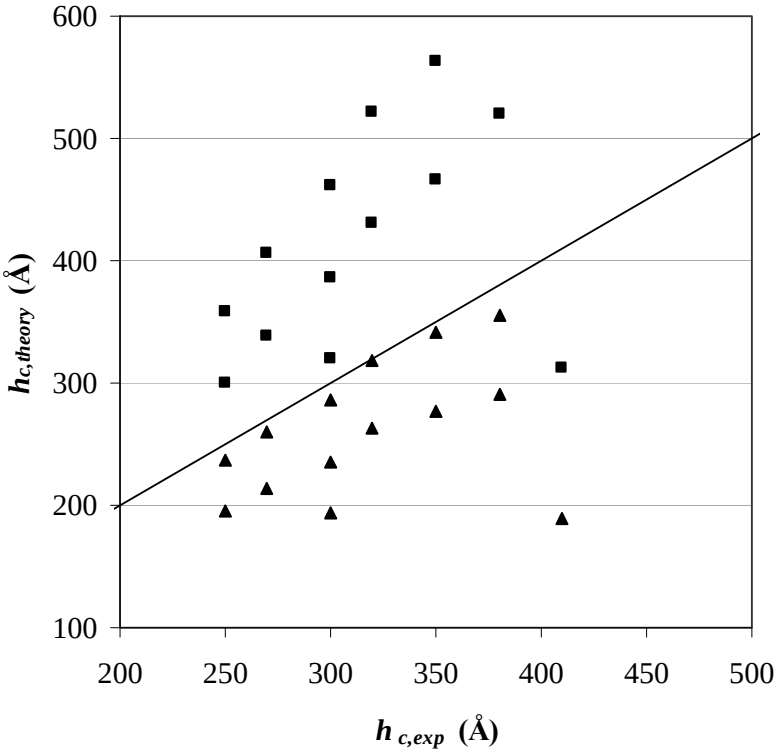
600
500
400
300
200
100
200
250
300
350
400
450
500
$h_{c,theory}$ (Å)
$h_{c,exp}$ (Å)

Figure 5.

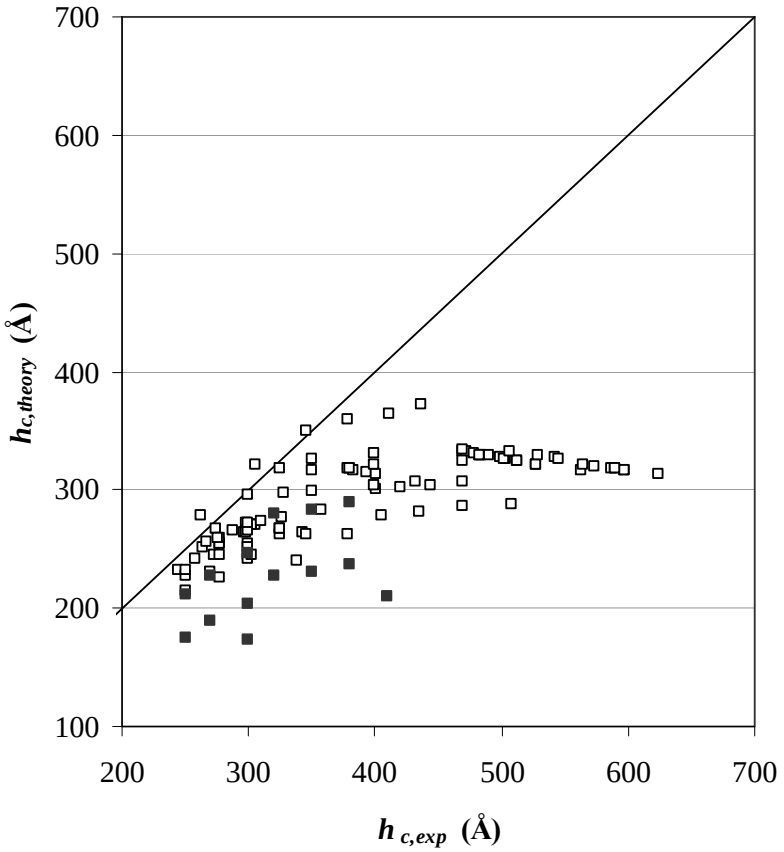
700
600
500
400
300
200
100
200
300
400
500
600
700
$h_{c,theory}$ (Å)
$h_{c,exp}$ (Å)

Figure 6.

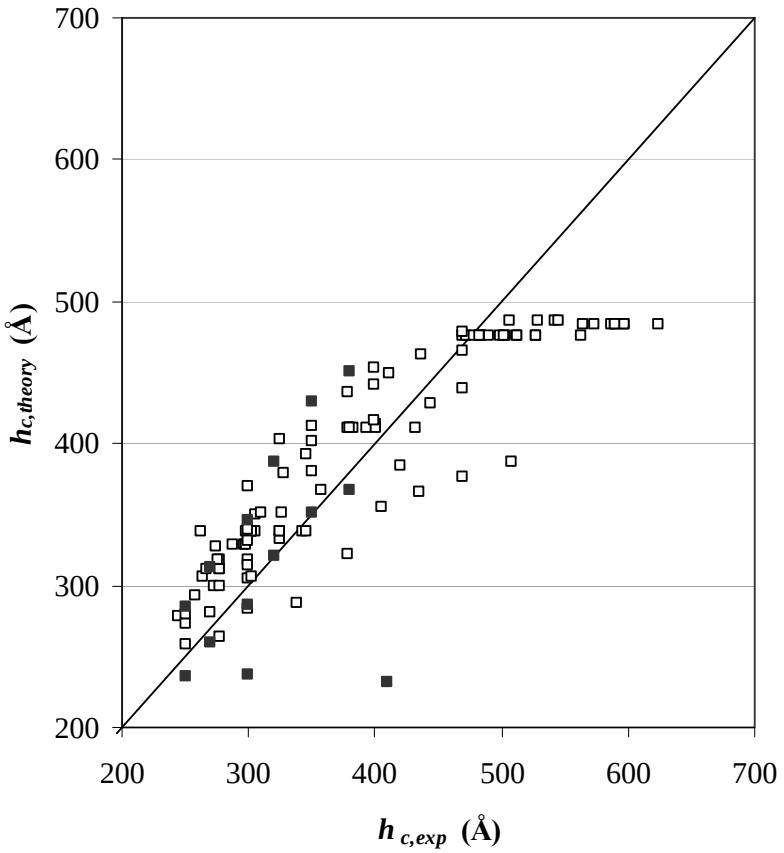
700
600
500
400
300
200
200
300
400
500
600
700
$h_{c,theory}$ (Å)
$h_{c,exp}$ (Å)

Figure 7.